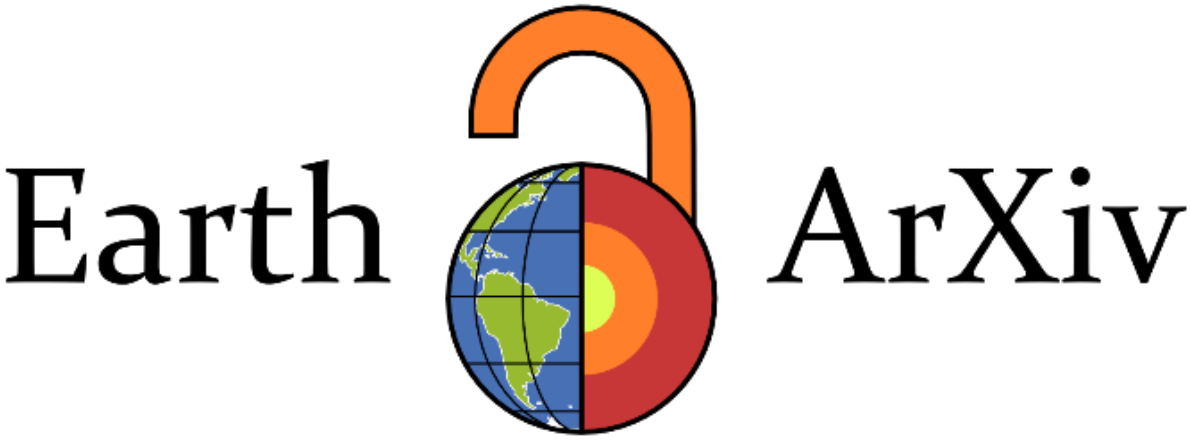

Development and Evaluation of the High-Resolution MUSICA UK Domain: A Case Study of Global and Regional Biomass Burning Impacts

Zhiyi Song[1], James A. King[2], Wenfu Tang[3], Jun Zhang[3], Haofan Wang[4], Louisa Emmons[3], James D. Allan[1], David O. Topping[1], Maria Val Martin*[2], and Zhonghua Zheng*[1]

[1]Department of Earth and Environmental Sciences, The University of Manchester, Manchester, M13 9PL, UK
[2]Leverhulme Centre for Climate Change Mitigation, School of Biosciences, The University of Sheffield, Sheffield, S10 2TN, UK
[3]Atmospheric Chemistry Observations & Modeling Laboratory, NSF National Center for Atmospheric Research (NCAR), Boulder, CO, USA
[4]School of Atmospheric Sciences, Sun Yat-sen University, Zhuhai 519082, China

*Email: zhonghua.zheng@manchester.ac.uk; m.valmartin@sheffield.ac.uk

Abstract

Regional air quality models provide insights into local pollution and exposure, but limitations in representing large-scale atmospheric processes and long-range transport can introduce inconsistencies across spatial scales, which can be addressed using multi-scale chemical transport models. We develop the first UK-specific regionally refined grid (UKne30×16; ∼7 km), alongside a global uniform grid (ne60; ∼56 km), within the Multi-Scale Infrastructure for Chemistry and Aerosols version 0 (MUSICAv0), and evaluated against in situ observations and reanalysis data. MUSICAv0 reproduces the spatial patterns of annual mean surface O_3 (R = 0.87; NMB = 12.80%) and $PM_{2.5}$ (R = 0.64; NMB = -15.70%) across the UK. Compared with ne60, the UK refined configuration better represents transboundary pollution transport, resolves fine-scale horizontal dispersion and vertical mixing, and more accurately captures the spatial variability during pollution episodes. Using biomass burning (BB) as case studies, we show that long-range BB transport elevates springtime $PM_{2.5}$ by 15–25% and O_3 by 5–8%, while summer enhancements of ∼10–14% are associated with local BB emissions, highlighting the importance of non-domestic emissions for UK air quality. Further analysis of the 2018 Saddleworth Moor wildfire shows MUSICAv0's ability to resolve plume transport and vertical structure, with wildfire smoke extending to ∼5.5 km altitude and significantly degrading air quality.

1. INTRODUCTION

Air pollution remains a critical global health risk factor, contributing to disease burden and premature mortality.[1–3] In the UK, approximately 29,000 to 43,000 deaths annually are attributable to poor air quality,[4,5] drawing increasing attention to pollution sources that can influence air quality. One such source is biomass burning (BB). It emits large amounts of aerosols and trace gases including primary organic aerosols (POA), volatile organic compounds (VOCs), and nitrogen oxides (NO_x). These compounds undergo complex chemical transformations in the atmosphere,[6–8] leading to the formation of secondary pollutants, such as tropospheric ozone (O_3) and secondary organic aerosols (SOA), a major contributor to fine particulate matter ($PM_{2.5}$; particles smaller than 2.5 μm).[9,10] BB is therefore widely recognized as a major source of both local and regional air pollution across many regions of the world, especially in Southeast Asia, Australia, North America and Northern Europe.[11–14] Through long-range transport, BB plumes can also deteriorate air quality far from the emission source, affecting downwind regions and even other countries.[15–17]

These issues are becoming increasingly relevant for the UK as large wildfire events are becoming more frequent and intense in key upwind regions, such as Canada, the western United States, and the Mediterranean basin, driven by rising temperatures and more persistent drought conditions.[18–20] These fires can inject large quantities of smoke into the free troposphere,[21] enabling long-range transport of BB pollutants across the North Atlantic and into Europe.[18,22,23] The UK has already experienced episodes of intrusions of wildfire smoke aloft from such events, with long-range transport contributing up to 1 $\mu g/m^3$ ($\sim$10%) to annual mean $PM_{2.5}$.[24] At the same time, the UK is primarily subject to moorland and peatland fires, and domestic wildfire activity has increased in recent years in response to intensifying climate extremes.[25,26] The Saddleworth Moor fire provides a recent example of a large event that affected regional air quality, during which $PM_{2.5}$ concentrations in the Manchester area increased by 150–200%, with daily mean levels reaching about 4–5.5 times the seasonal average.[27] This event was associated with an estimated 8.6 excess deaths and £21.1 million in health related economic losses.[28] These trends highlight the need for modeling tools capable of assessing the impacts of remote and local BB sources on UK air quality.

Atmospheric chemistry transport models are widely used to investigate BB air pollution and commonly used regional air quality models across Europe include the Weather Research and Forecasting model coupled with Chemistry (WRF-Chem),[29] the European Monitoring and Evaluation Program (EMEP) model,[30] the Comprehensive Air Quality Model with Extensions (CAMx),[31] and the Community Multiscale Air Quality (CMAQ) model.[32] Local-scale dispersion models such as the Atmospheric Dispersion Modeling System (ADMS) are commonly applied to quantify near field air quality impacts and are not designed to represent regional-scale transport or detailed atmospheric chemistry.[33] While these regional and local-scale models are capable of resolving air pollution processes at relatively finer spatial resolution, they typically require boundary and initial conditions from global climate models (GCMs), Earth system models (ESMs), or reanalysis datasets.[34,35] Discrepancies in spatial resolution, physical parameterizations and chemical mechanisms between regional models and GCMs/ESMs can introduce inconsistencies and add uncertainty to simulated pollutants.[36,37] Such challenges complicate the representation of climatic processes, long-range transport and chemical processes that influence regional air quality.[37–39]

Variable resolution (VR) grids within GCMs/ESMs offer an alternative. By operating within a unified modeling framework with internally consistent dynamics and physical parameterizations, VR configurations allow regional domains to be refined within a global model while maintaining consistent physics and chemistry across resolutions. This approach reduces boundary artifacts and resolution mismatches,[40,41] enables two-way interactions across global and regional scales, and has been shown to improve simulations of regional climate in areas with complex topography.[42]

The Multi-Scale Infrastructure for Chemistry and Aerosols (MUSICA) is a state-of-the-art unified modeling framework built within Community Earth System Model (CESM) that allows global to regional atmospheric chemistry and aerosols simulations using VR configuration.[43] Recent applications of MUSICAv0 over continental US, Africa, South America and East Asia show that higher spatial resolution combined with updated chemical mechanisms improve model performance and representation of air pollutants, BB plumes and atmospheric processes.[44–47] For example, Jo et al. (2023) showed that regional refinement to $\sim$7–14 km in MUSICAv0 substantially improves chemical fields (OH, O_3, NO_3), with boundary layer concentration differing by up to an order of magnitude, and high-resolution grids reproducing aircraft observations more accurately than coarse global grids.[47] However, previous applications of MUSICAv0 have generally used spatial resolution of 14–28 km, and no study to date has developed a high-resolution MUSICA domain for the UK. While several studies have examined the BB impacts on UK air quality, these impacts have not yet been explored using a unified multi-scale framework.

To address this gap, we develop a new MUSICAv0 configuration featuring a regionally refined grid ($\sim$7 km) over the UK domain nested within a global uniform grid ($\sim$110 km), and compare it with a separate global uniform grid configuration ($\sim$56 km). We conduct simulations to evaluate the added value of the UK refined domain in capturing atmospheric processes and to quantify both global and regional BB impacts on UK air quality as a case study. This work provides a valuable first study toward applying MUSICAv0 for high-resolution air quality assessment in the UK and highlights the important role of BB in shaping regional air quality.

2. METHODS

2.1 Model Overview

Simulations are conducted using MUSICAv0, a configuration of CESM2.2 that couples the atmosphere, land, sea ice and other Earth system components.[48] MUSICAv0 employs the hydrostatic Spectral Element (SE) dynamical core, implemented on a cubed-sphere grid within the Community Atmosphere Model (CAM).[49] The SE has been tested in CESM2 and serves as the default dynamical core for high-resolution CESM2 applications.[36] In MUSICAv0, the CAM with Chemistry (CAM-Chem)[50,51] is coupled with the SE dynamical core, enabling regional refinement (RR) down to a few kilometers through using variable-resolution grids (CAM-Chem-SE-RR/MUSICAv0).[52,53] The model is configured with 32 vertical layers extending to 3.64 hPa. Approximately 7 layers are located below the planetary boundary layer height (PBLH; below 850 hPa), and around 15 layers are positioned in the stratosphere and above (above 200 hPa). A hybrid sigma-pressure vertical coordinate is used to accommodate surface topography. The planetary boundary layer, shallow convection, and cloud macrophysics are represented by the Cloud Layers Unified by Binormals (CLUBB) scheme.[54,55] Cloud microphysical processes are simulated using the MG2 scheme,[56] which is coupled to the four-mode version of the Modal Aerosol Module (MAM4).[57] Deep convection is parameterized using the McFarlane (ZM) scheme.[58] To simulate land processes and the deposition of gases and aerosols, MUSICAv0 is interactively run with the Community Land Model version 5 (CLM5).[59] MUSICAv0 supports multiple chemical mechanisms with different complexity. In this study, MOZART-TS2 chemical mechanism (Model for Ozone And Related chemical Tracers with troposphere-stratosphere v2) is used, providing comprehensive tropospheric and stratospheric chemistry with a more detailed representation of isoprene and terpene oxidation.[60]

2.2 Development of the UK Regionally Refined Grid

We developed a regionally refined grid over the UK to enable high-resolution and air quality studies within the MUSICA framework (Figure 1 and Figure S1). In this study, we use this grid to assess the impacts of global BB on regional air quality. The "ne" resolution label refers to the number of elements along each coordinate direction of a cube face.[49] Starting from a standard ne30 (approximately 1°, ∼111 km) cubed-sphere grid, we apply a rotational transformation to position the UK at the center of one cube face. A regional refinement is then created over the UK at a resolution of ne30×16 (approximately 1/16°, ∼7 km), hereafter referred to as UKne30×16, while the rest of the globe remains at the original ne30 resolution.

For the global ne60 uniform grid (approximately 1/2°, ∼56 km), we apply a similar rotational transformation to center the UK on one cube face, after which each face is refined into 60×60 spectral elements. In the final step of UKne30×16 and ne60 grids setup, each element is placed with a 4×4 Gauss-Legendre-Lobatto (GLL) quadrature points to enable the representation of third-order Legendre basis functions.[61]

To mitigate potential numerical errors arising from abrupt resolution transitions within short distances, a halo zone is introduced in UKne30×16, allowing for a smooth transition between the finer and coarser regions. Following the recommendations from Herrington and Reed (2020),[62] the UKne30×16 grid uses a physical timestep of 225 seconds and a dynamical timestep of 18.75 seconds, the ne60 grid uses timesteps of 900 seconds and 150 seconds, respectively, to ensure model stability. Although both grids use the same dynamical core, chemical mechanism and physics package, the resulting meteorological and chemical fields may differ due to the differences in horizontal grids and computational time steps.

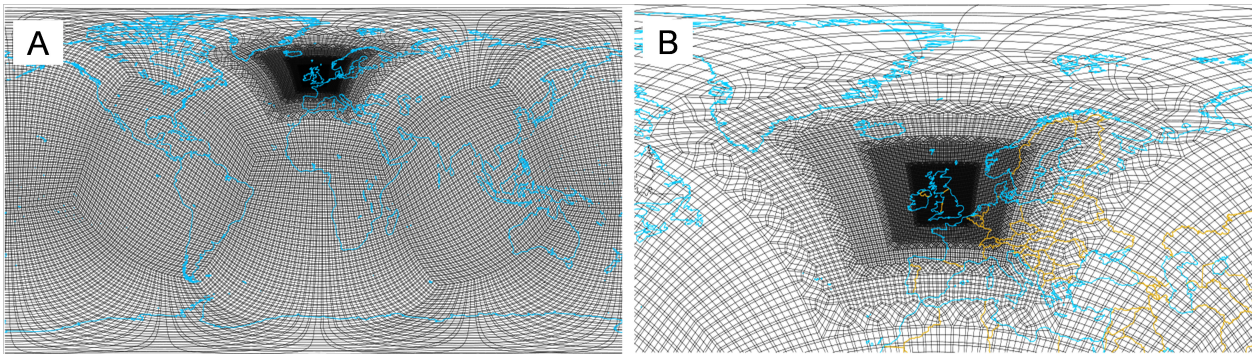

Figure 1: Variable resolution grid developed across the UK with MUSICAv0. (A) The UKne30×16 grid, with regional refinement over the UK at 1/16° (∼7 km), while the rest of globe remains at 1° (∼111 km). (B) Zoomed view over the UK showing the halo zone between the refined and coarse resolution regions.

2.3 Model Simulations Setup

The MUSICAv0 simulations use both online and offline emissions. Biogenic emissions are calculated online using the MEGANv2.1 (Model of Emissions of Gases and Aerosols from Nature v2.1)[63] within CLM5. Biogenic VOC emission fluxes are estimated using CLM5 specified phenology (SP) configuration, where vegetation phenology and leaf area index (LAI) are prescribed. Sea salt and dust emissions are likewise computed online. Lightning NOx emissions are calculated online using the parameterization of Price et al. (1997).[64] All other emissions are applied offline. Global anthropogenic emissions are from Copernicus Atmospheric Monitoring System Global Anthropogenic Emissions version 5.1 (CAMS-GLOB-ANTv5.1) which is available at $0.1^\circ \times 0.1^\circ$ spatial resolution. CAMS-GLOB-ANTv5.1 is based on the Emissions Database for Global Atmospheric Research Version 5 (EDGARv5)[65] up to 2015, with emissions for 2016–2021 extrapolated using the Community Emissions Data System (CEDS).[66] Aircraft emissions are from the CAMS-GLOB-AIRv2.1,[67] which provides emissions at spatial resolution of $0.5^\circ \times 0.5^\circ$. In this study, black carbon (BC), NO_2 and SO_2 are used from this aircraft inventory following the approach of Jo et al. (2023).[47] BB emissions are estimated from Quick Fire Emissions Dataset (QFED) v2.5_r1[68] and Fire Inventory from NCAR (FINN) v1.5.[69] Emissions for the chemical species required for MUSICAv0 are generated by scaling QFED CO_2 emissions with FINN aerosol and trace gas emission factors. Emissions from ocean and soil sources are derived from the Chemistry Climate Model Initiative (CCMI).[70] All offline emissions are regridded to the UKne30×16 and ne60 grids using the first-order conservative method,[71] in order to better resolve fine-scale emission features and minimize artificial dilution of concentrated emissions.[53]

Separate land and atmospheric spin-ups are conducted to generate initial conditions. For the land spin-up, the CESM2.2 (with CLM5) model is run for five years on the UKne30×16 and ne60 grids using a reduced chemical mechanism.[47] For the atmospheric spin-up, the CESM2 is run with CAM-Chem model with the MOZART-TS1 chemical mechanism on a 1° finite-volume grid for one year to ensure sufficient spin-up time for long-lived species.[50] The output is then conservatively regridded to the UKne30×16 and ne60 grids. A final three month spin-up (September 1–November 30, 2017) is performed for MUSICAv0, initialized with the spun-up land fields and regridded atmospheric fields. A summary of simulations and configurations used in this study can be found in Table 1. Production simulations then run for one full year (December 1, 2017–November 30, 2018). All MUSICAv0 simulations use identical dynamical cores, physical parameterizations, and chemical mechanisms. The production simulations focus on 2018 because it includes the largest wildfire on record in the UK (the Saddleworth Moor wildfire)[27] and represents a year with relatively low global BB emissions during 2002–2020,[72] allowing the simulated BB impacts to be interpreted as a conservative estimate of global BB influence.

Meteorological fields including temperature (T), zonal wind velocity (U) and meridional wind velocity (V), are nudged to Modern-Era Retrospective Analysis for Research and Applications Version 2 (MERRA2)[73] with a relaxation time of 12 hours to maintain consistency with large-scale conditions. For UKne30×16 grid, nudging is not applied within the refined region, as its resolution (∼1/16°) exceeds that of MERRA2 ($0.67^\circ \times 0.5^\circ$), which helps preserve the high-resolution meteorological features.[47] Two simulations are designed to

Table 1: Summary of model simulations and configurations.

Grid	Simulation label	Impacts of BB	Nudging configuration
UKne30×16	ne30×16	On	Window nudged[a]
	BB_ne30×16	On	Window nudged[a]
	NOBB_ne30×16	Off	Window nudged[a]
ne60	ne60	On	Global nudged[b]

Note: [a]Nudging is not applied within the refined region, while outside the refined region the nudging is consistent with that used in the ne60 configuration. [b]Nudging is applied at global scale.

evaluate MUSICAv0's capability to capture global and regional BB impacts on air quality in the UK. These simulations also serve as an initial test of the new UK regional refinement domain within MUSICAv0. Both simulations use the UKne30×16 grid: BB_ne30×16 and NOBB_ne30×16, with and without BB, respectively. For comparison, ne60 simulations are run for the same period as BB_ne30×16, serving as control runs to quantify the added value of regional refinement.

2.4 Observations and Reanalysis Datasets for Model Evaluation

Independent observations are essential for assessing how well models reproduce real world air pollution concentrations. To evaluate the performance of MUSICAv0 over the new UK regional refinement domain, we use observations from the Automatic Urban and Rural Network (AURN; `https://uk-air.defra.gov.uk/networks/network-info?view=aurn`). The AURN is the largest automated air quality monitoring network in the UK with over 190 sites nationwide. Operated by the Department for Environment, Food and Rural Affairs (DEFRA), the network continuously measures air pollutants using standard methods specified by the European Commission. AURN data undergo a three-stage quality assurance process, including automatic uploading from monitoring sites, manual validation and quarterly ratification, to ensure data accuracy and compliance with national QA/QC standards before datasets are released as verified observations.

Hourly observations of surface $PM_{2.5}$ and O_3 are used to evaluate the spatiotemporal performance of MUSICAv0. Comparisons between MUSICAv0 simulations and observations are conducted for four major UK cities (Glasgow, Manchester, Birmingham, and London), which span a north-south latitudinal gradient and are selected to represent major UK urban pollution hotspots. We examine the temporal evolution of $PM_{2.5}$ and O_3 in each city and assess the spatial distribution of concentrations across all monitoring sites against the model fields. The analysis covers the period from December 1, 2017 to November 30, 2018, with additional temporal evaluations conducted during May and June 2018. Observed maximum daily 8-hour average (MDA8) ozone is calculated from hourly O_3 measurements.

The UK Air Quality Reanalysis provided by the Met Office (UKAQR; `https://air-quality-1-themetoffice.hub.arcgis.com/pages/explore-data`) combines an air quality forecasting model with pollutant observations to produce an enhanced representation of past pollutant concentrations across the UK. Monthly average $PM_{2.5}$ and O_3 concentrations gridded at 0.1° from December 2017 to November 2018 are used to further evaluate the spatial performance of MUSICAv0 by providing spatial distributions that complement the point-based AURN observations.

3. RESULTS

3.1 Overall Evaluation of the Regionally Refined Grid

The overall performance of MUSICAv0 regional grid is evaluated by comparing UKne30×16 simulations for the period November 2017–December 2018 against the UKAQR (Figure 2). The UKne30×16 simulation outputs are regridded to the 0.1° UKAQR grid using the first-order conservative method.[71] Spatial distribution of surface O_3 and $PM_{2.5}$ simulated by MUSICAv0 over the UK are broadly consistent with UKAQR. Both MUSICAv0 and UKAQR exhibit a marked latitudinal gradient in surface O_3, with higher concentrations over the northwestern UK, including northern Scotland and Northern Ireland, and lower concentrations across the more highly populated southeastern regions (Figure 2a–b). MUSICAv0 slightly overestimates

surface O_3, with a mean bias of 7.57 $\mu g/m^3$ (NMB = 12.80%), which is comparable to previous MUSICAv0 applications (∼11–29%),[74] while still capturing the spatial pattern of annual average O_3 well (R = 0.87). The model performs best in spring for surface O_3, with a mean bias of 3.40 $\mu g/m^3$ (NMB = 5.38%) and a strong correlation with UKAQR (R = 0.92) (Figure S2).

MUSICAv0 and UKAQR exhibit a similar spatial pattern of surface $PM_{2.5}$, with elevated concentrations in southeastern UK and lower levels in the northwest. However, MUSICAv0 tends to underestimate surface $PM_{2.5}$ in the southeast, especially over London and the southern coastal regions, by approximately 2–4 $\mu g/m^3$ (Figure 2e–g). This underestimation becomes more pronounced during spring (Figure S2). Despite this bias, MUSICAv0 captures the spatial pattern of annual average $PM_{2.5}$ reasonably well (R = 0.64), with a mean bias of 1.04 $\mu g/m^3$ (NMB = -15.70%; Figure 2h), which is at the lower end of biases reported in previous MUSICA applications (∼1–10 $\mu g/m^3$).[46,52] MUSICAv0 performs unevenly across the domain, with better agreement with UKAQR for surface $PM_{2.5}$ in the western UK (west of 3°W; R = 0.64 and MB = 0.47 $\mu g/m^3$) and larger discrepancies in the eastern UK (east of 3°W; R = 0.61 and MB = -2.39 $\mu g/m^3$) (Figure 2h). These differences likely reflect two distinct $PM_{2.5}$ regimes across the UK. The western UK is more frequently influenced by clean marine air masses from the North Atlantic, which are better captured by MUSICAv0, whereas the eastern region is more affected by pollution transported from continental Europe. In addition, higher local NO_x emissions associated with greater population density in the east further contribute to the underestimation because inorganic nitrate aerosols are not included in the current version of MAM4 used in MUSICAv0.[57,75] Nitrate and ammonium aerosols are key precursors of $PM_{2.5}$.[76,77]

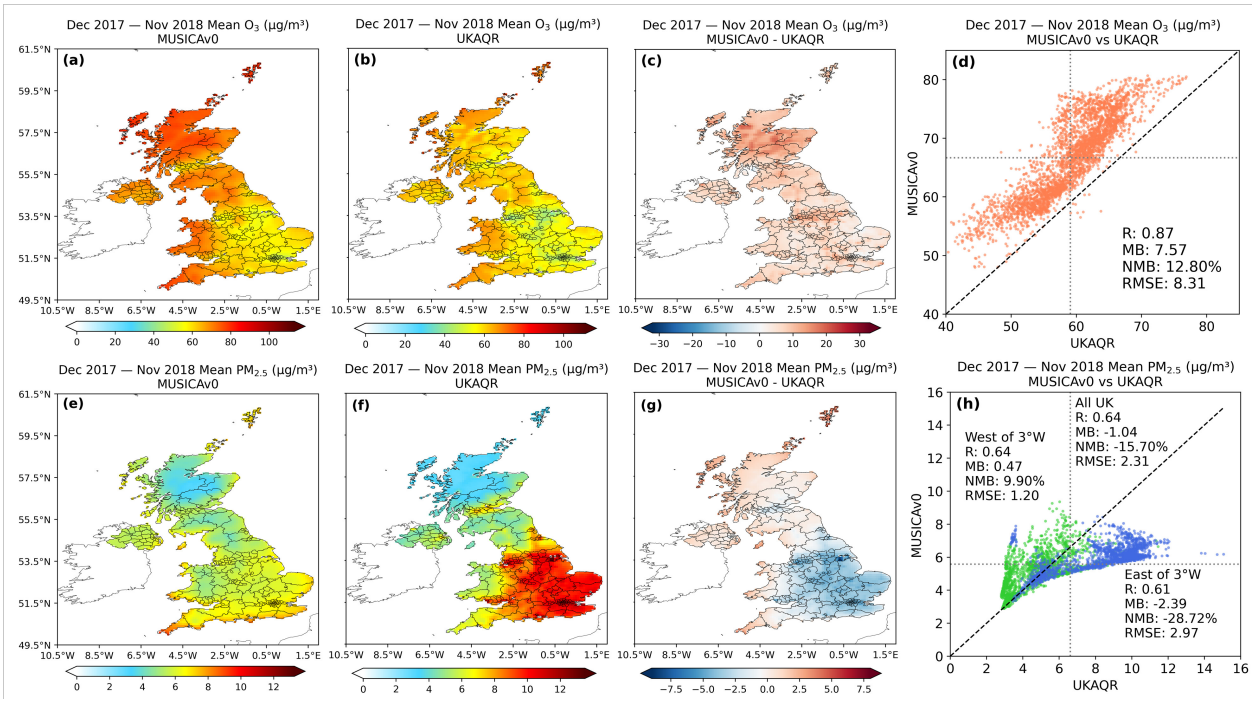

Figure 2: Comparison of annual average surface O_3 and $PM_{2.5}$ concentrations simulated by MUSICAv0 from December 2017 to November 2018 with the UK Air Quality Reanalysis (UKAQR) with MUSICAv0 (a, e), UKAQR (b, f), and difference between MUSICAv0 and UKAQR (c, g) and scatter plot of O_3 and $PM_{2.5}$ concentrations comparing UKAQR and MUSICAv0 (d, h). Dashed vertical and horizontal lines indicate mean values of UKAQR and MUSICAv0. Green points represent grid cells west of 3°W, while the blue points correspond to those east. MUSICAv0 output is conservatively regridded to the 0.1° UKAQR grid.

3.2 Evaluation during an Intrusion Event from Continental Europe

The added value of the MUSICAv0 regional grid is evaluated by comparing UKne30×16 and ne60 simulations during a late-spring European continental pollution intrusion against AURN observations (Figure 3). These

episodes are common in the UK and have been shown to contribute 20–60% of UK springtime $PM_{2.5}$ nitrate under persistent high-pressure conditions[78] and offer a valuable opportunity to evaluate model skill in representing long-range transport and associated meteorology. Accordingly, we use one such event as a test case. In this study, the start of the intrusion is defined as the day when near-surface winds shift from prevailing westerly-southwesterly to easterly-southeasterly flow, and it ends when westerly-southwesterly winds become dominant again. This definition focuses on the large-scale circulation change that facilitates the transport of polluted air masses into the UK.

Both grids reproduce the observed spatial distributions of $PM_{2.5}$ and O_3 during the intrusion period, but tend to underestimate $PM_{2.5}$. The skewness (Sk) of $PM_{2.5}$, which reflects the model's ability to capture the asymmetry and extremity of concentration distributions during episodic events, is calculated for both grids. Compared to ne60 (Sk = 1.75–3.05), UKne30×16 produces lower Sk values (Sk = 1.49–2.46) that more closely aligns with AURN observations (Sk = 1.06–1.92), indicating an improved ability to capture the $PM_{2.5}$ variability during the intrusion event (Figure S4). Additionally, UKne30×16 also demonstrates improved performance in simulating O_3 variability, particularly in Glasgow, where the NMB is 6.5%, MB is 2.1 ppbv and the maximum bias is reduced to approximately 15 ppbv (Figure 3c and Figure S5). In contrast, ne60 shows larger positive biases likely as a result of mixing effects of emissions from surrounding regions (Figure 3c and Figure S6). Many of the finer features captured by UKne30×16 persist even after regridding to the ne60 grid (Figure S3).

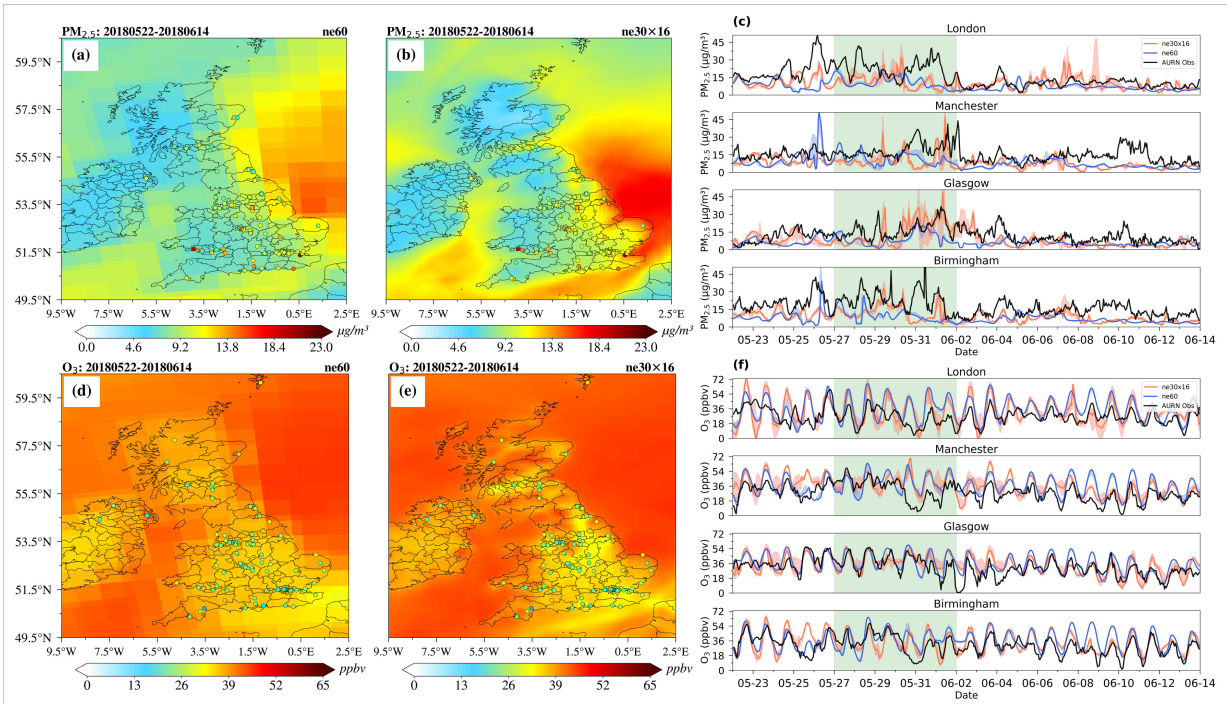

Figure 3: Comparison of MUSICAv0 simulations with AURN observations during a late-spring pollution intrusion event (22 May to 14 June 2018). Spatial distribution of average $PM_{2.5}$ and O_3 for ne60 (a and d) and UKne30×16 (b and e) with AURN observations shown as filled dots. Daily variations of $PM_{2.5}$ (c) and O_3 (f) in four key UK cities, with simulations shown in blue (ne60) and red (UKne30×16) and AURN observations in black. Shaded bands around the model lines surrounding red and blue lines indicate the concentration ranges across the grid cells containing observation sites. Green shading marks the peak intrusion period.

Our study domain is 9°W–9°E, 49.5°N–61.5°N, selected as it covers the British Isles and the North Sea and captures both national emission sources within the UK and the primary transboundary transport pathways from Europe. Across this domain, both simulations produce generally consistent meteorological fields in terms of temporal variability (Figure S7). The closest agreement is found in downwelling solar flux

and PBLH, whereas large discrepancies appear in cloud fraction and precipitation. To assess the effect of meteorological differences on chemical species, BC serves as a proxy because of its chemical inertness and dominant role of meteorology in controlling its surface concentrations.[47] Compared with ne60, UKne30×16 shows a BC NMB of 2.3% over the evaluated domain and period, indicating that meteorological differences between the two grids have a limited impact on surface BC (Figure S7).

The regionally refined grid (UKne30×16) captures better fine-scale variations of $PM_{2.5}$ in both the horizontal and vertical directions. Figure 4 shows the simulated spatial transport of $PM_{2.5}$ during the peak intrusion period for UKne30×16 and ne60. The UKne30×16 simulation generally produces higher surface $PM_{2.5}$ concentrations than ne60 and better resolves small-scale thermodynamic stability in the lower troposphere (Figure S8). On 27 May, both grids simulate similar wind speeds, but UKne30×16 captures a weak anticyclonic circulation over southern England that enhances subsidence and elevates $PM_{2.5}$, whereas ne60 simulates elevated $PM_{2.5}$ farther east (Figure 4a, 4e and Figure S8). On 28 and 29 May, the simulations diverge more substantially: UKne30×16 simulates stronger northeasterly winds and higher wind speeds, while ne60 produces weaker easterly winds at the surface (Figure 4bc and 4fg). These discrepancies may reflect improved representation of vertical mixing processes in UKne30×16. Over southern England, UKne30×16 resolves a notable temperature inversion near 900 hPa, which inhibits vertical mixing and contributes to surface $PM_{2.5}$ accumulation, whereas ne60 does not capture this inversion (Figure S8). On 30 May, both grids capture the inversion, but ne60 shows stronger ascending motion over the most polluted area, enhancing vertical mixing and reducing surface $PM_{2.5}$ concentrations (Figure 4d, 4h and Figure S8). In summary, UKne30×16 provides a more realistic simulation of pollution intrusion by better resolving fine–scale horizontal dispersion and vertical mixing.

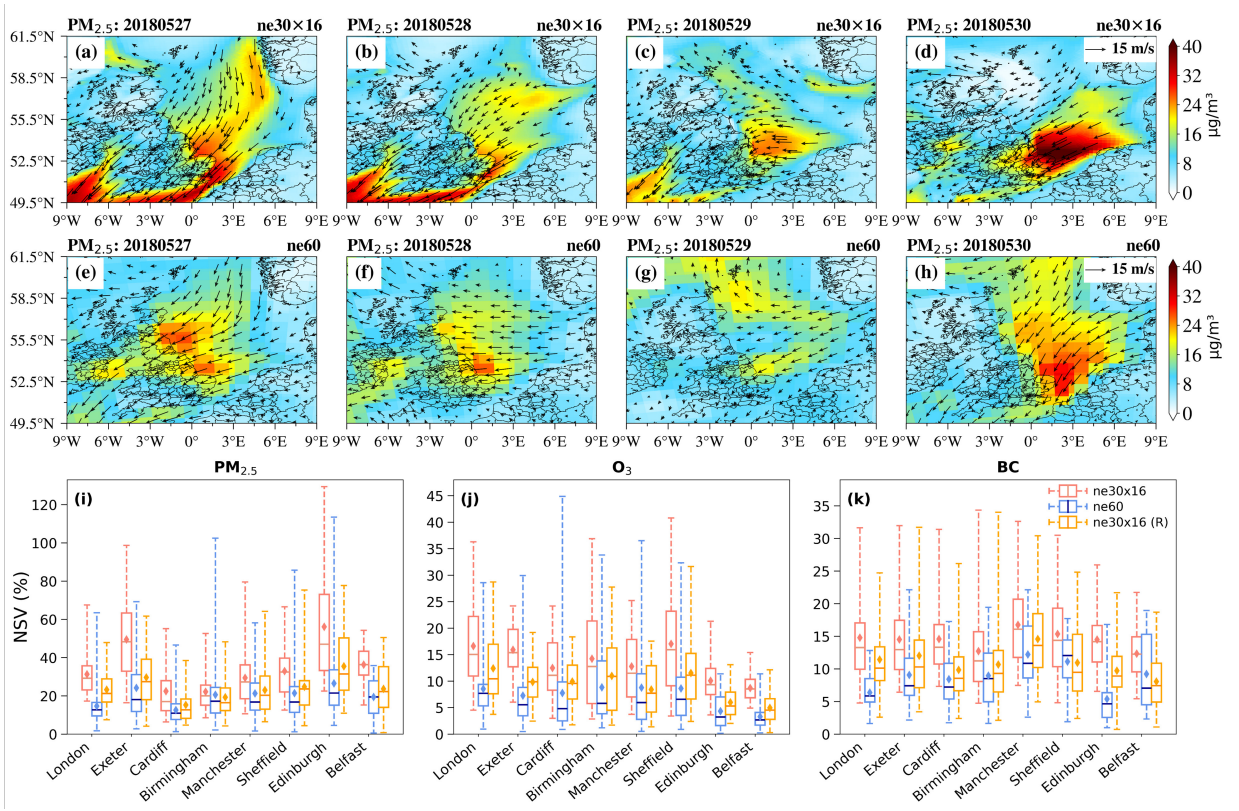

Figure 4: Comparison of UKne30×16 and ne60 simulations during peak pollution intrusion (27–30 May 2018). Panels (a–h) show simulated average daily surface $PM_{2.5}$ concentrations ($\mu g/m^3$) and surface wind vectors for ne30 × 16 and ne60 over the domain 9°W–9°E, 49.5°N–61.5°N. Panels (i–k) present boxplots of the normalized spatial variability (NSV; %) at the surface for $PM_{2.5}$, O_3, and black carbon (BC) across selected cities. Results from ne30 × 16 are shown in red, ne60 in blue, and ne30 × 16 regridded to ne60 in yellow.

To further quantify the added value of the regionally refined grid, we analyze the normalized spatial variability (NSV) following the method in Tang et al.[52] Within the refined MUSICAv0 domain, $1^\circ \times 1^\circ$ boxes are centered on each selected city, and NSV is calculated as the ratio of the standard deviation to the mean of pollutant concentrations across all grid points within each box. Calculations are based on hourly data during the peak intrusion period. Figure 4i–k show NSV for surface $PM_{2.5}$, O_3, and BC, whereas NSV for surface temperature, precipitation, CO and wind (u, v) is shown in Figure S9. In terms of median NSV, UKne30×16 shows increases of 8–20% for $PM_{2.5}$ and 5–10% for O_3, compared to ne60. When UKne30×16 simulations are regridded conservatively to ne60,[71] median NSV still remains higher. Despite the limited influence of meteorological differences on surface BC, UKne30×16 still increases surface BC NSV by up to approximately 7%. After regridding to ne60, this improvement remains evident in most cities, except Sheffield and Belfast, where ne60 shows greater spatial variability in meridional winds (Figure S9), which enhances the BC variability. Overall, UKne30×16 simulates higher NSV, indicating an improved capability to resolve variability at regional scales.

3.3 Global Biomass Burning Impacts on UK Air Quality

We further demonstrate the capability of MUSICAv0 over the UK domain through a case study assessing the impacts of global BB on UK air quality. Seasonal BB impacts on regional $PM_{2.5}$ and O_3 are quantified by comparing simulations from the BB and NOBB scenarios, with evaluation against AURN observations (Figure S10–S12). The fractional enhancement due to BB is calculated as the relative difference between $BB_{ne30\times16}$ and $NOBB_{ne30\times16}$, normalized by $NOBB_{ne30\times16}$.

Spatially, both scenarios reproduce distributions consistent with the AURN observations (Figure 5 and 6). In spring (Figure 5f), $PM_{2.5}$ concentrations typically reach 10–13 $\mu g/m^3$, with localized enhancements exceeding 16 $\mu g/m^3$ in the London areas. Scotland and the eastern UK coast show strong responses to BB transported from continental Europe, with fractional enhancements of 15–25% in Glasgow and Edinburgh, and over 25% near St Andrews (Figures 5g and 5h). These increases correspond to direct BB contributions of about 2 $\mu g/m^3$. This pattern is consistent with prevailing southeasterly winds during spring, which facilitate long-range transport from Europe (Figure 5h). In summer, with prevailing winds shifting to southwesterly and wind speed decreasing over central England (Figure 5l), the areas most affected shift toward central England and the southeastern coast, where fractional enhancements typically range from 10–17%, reaching up to around 20% in regions such as Nottingham and Birmingham (Figure 5k). The seasonal sensitivity of $PM_{2.5}$ to BB influence is also consistent with Tan et al. (2025),[24] which report pronounced springtime BB-driven pollution episodes from continental Europe, and sustained summer contributions from a combination of long-range transport and local BB emissions. Averaged over 2018, BB increases annual mean surface $PM_{2.5}$ across the UK by approximately 0.7 $\mu g/m^3$.

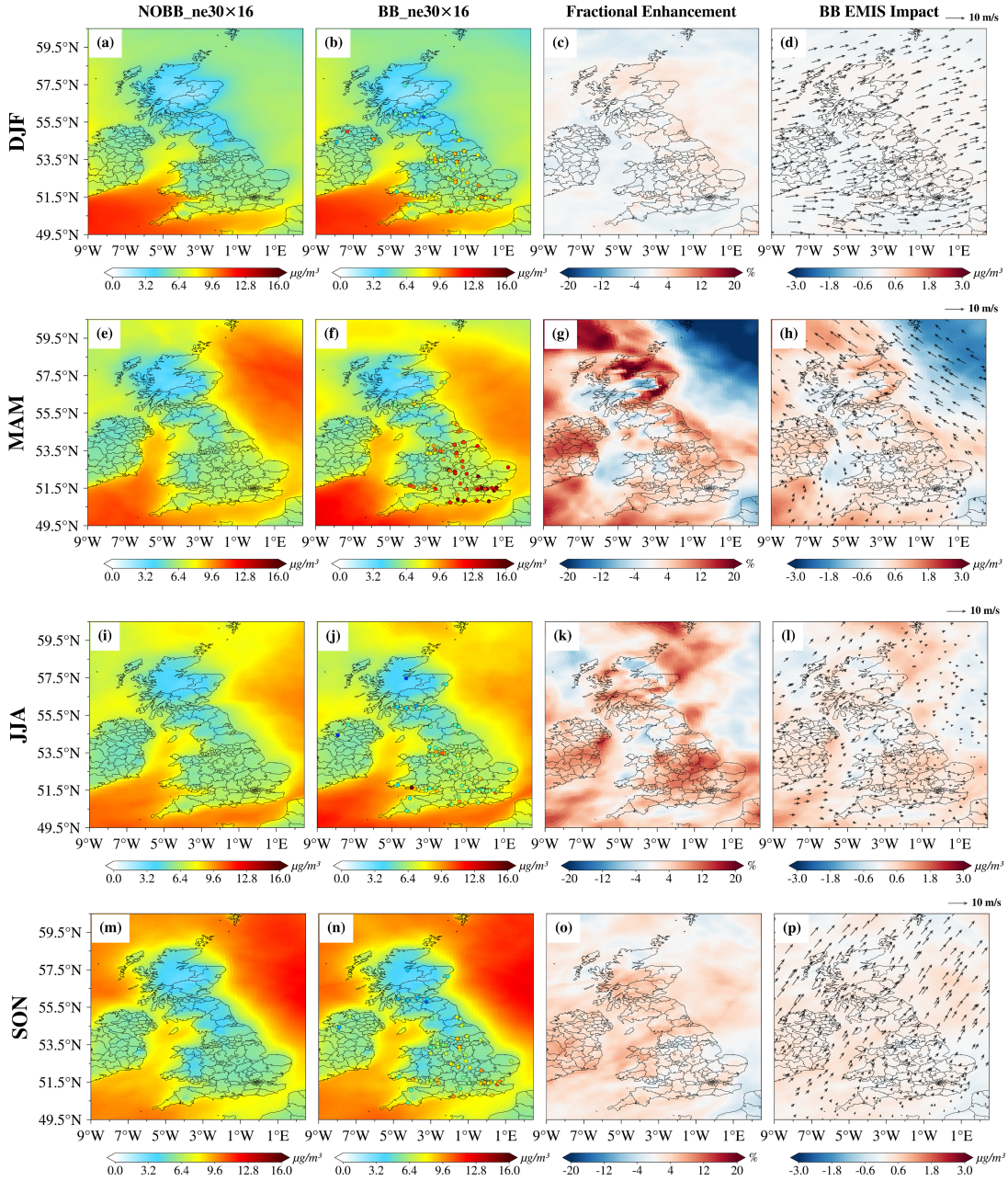

Figure 5: Spatial distribution of seasonal mean surface $PM_{2.5}$ ($\mu g/m^3$) over the UK from UKne30×16 simulations under scenarios with biomass burning (BB_ne30×16) and without biomass burning (NOBB_ne30×16), the fractional BB-induced enhancement, and the absolute BB contribution with wind vectors (u, v). Filled dots show AURN observations for the corresponding period.

Surface O_3 concentrations are higher in rural regions with low population density like northern Scotland and northern England, whereas urban areas with dense populations and higher traffic emissions show lower concentrations. This pattern is particularly evident in winter (Figure 6b), consistent with previous studies.[79,80] Reduced daylight hours during winter inhibit NO_2 photolysis, thereby limiting photochemical O_3 production. In rural and remote regions with low NO_x emissions, reduced O_3 titration allows background O_3 transported from the North Atlantic to persist. The direct impact of BB on O_3 during winter is negligible,

and elevated O_3 levels appear to be influenced by prevailing westerly and southwesterly winds bringing O_3 and its precursors from the North Atlantic (Figure 6c and 6d). In spring, intensified northeasterly winds from continental Europe transport additional BB-produced O_3 toward the UK (Figure 6h). This transported O_3, combined with elevated background concentrations from winter accumulation, results in the highest seasonal O_3 concentrations (Figure 6f). Fractional enhancements of about 5–8% and direct contributions of about 4 ppbv are evident over northern Scotland and parts of eastern and southern England (Figure 6g and 6h).

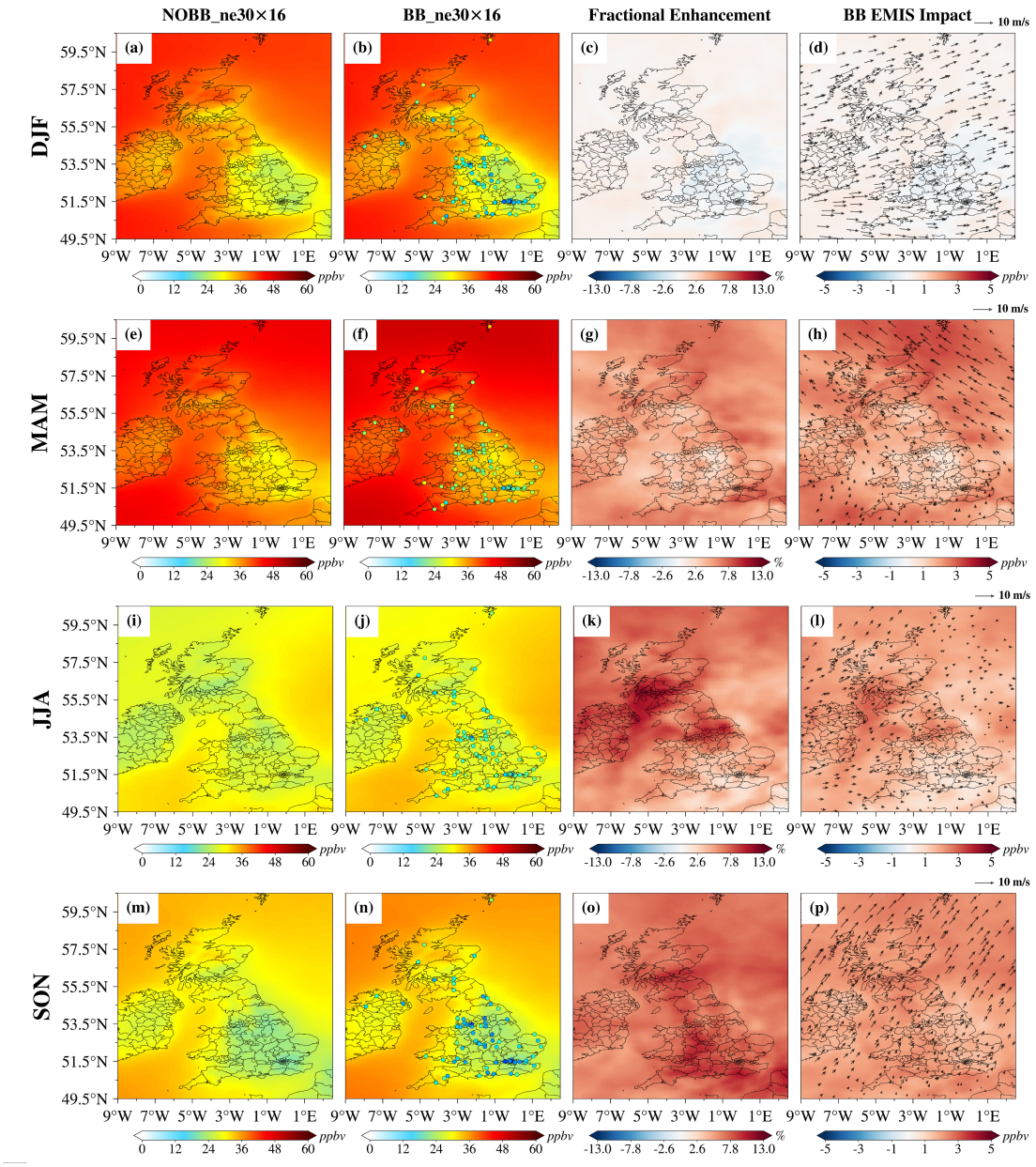

Figure 6: Spatial distribution of seasonal mean surface O_3 (ppbv) over the UK from UKne30×16 simulations under scenarios with biomass burning (BB_ne30×16) and without biomass burning (NOBB_ne30×16), the fractional BB-induced enhancement, and the absolute BB contribution with wind vectors (u, v). Filled dots show AURN observations for the corresponding period.

More pronounced changes of O_3 due to BB are observed in summer and autumn. In summer, factional enhancements are up to approximately 12–14% in northwestern England and western Scotland (Figure

6k), although overall O_3 concentrations remain at their lowest levels of all seasons (Figure 6j). These enhancements are primarily attributed to local BB events, including wildfires in northwestern England.[27] Prevailing southwesterly winds and reduced wind velocities limit long-range O_3 transport from Europe (Figure 6l). In addition, enhanced photolysis of O_3 over the North Atlantic during summer lowers the hemispheric background O_3 transported to the UK, and the associated increase in OH radicals from water vapor further accelerates chemical O_3 loss,[81] both contributing to the reduction in O_3 concentrations within the UK. During autumn O_3 concentrations gradually increase across the UK in autumn following the summer decline. Strengthened southwesterly winds expand BB-sensitive regions toward central Scotland as well as western and southern England, where fractional enhancements generally reach around 10–13% (Figure 6o and 6p). Compared with other seasons, autumn shows the largest overall UK-wide sensitivity to BB with fractional enhancements of approximately 6–9%.

3.4 Regional Biomass Burning Impacts on UK Air Quality

Building on the global scale analysis of BB impacts, we next evaluate MUSICAv0's ability to represent regional BB impacts through a high-resolution case study of the Saddleworth Moor fire. The Saddleworth Moor fire, which occurred during an exceptionally dry period in June 2018, is regarded as the largest wildfire recorded in English history.[27] Previous studies found $PM_{2.5}$ enhancements of approximately 150–200% over the Manchester area, with observed peak concentrations reaching 40–60 $\mu g/m^3$, while simulations conducted at a 12 km horizontal resolution reproduce $PM_{2.5}$ concentrations of about 15–30 $\mu g/m^3$.[27,28,82] Similar results are obtained in MUSICAv0 simulations at comparable resolutions, showing a $PM_{2.5}$ increase of about 133% over the Manchester area but underestimating peak $PM_{2.5}$ ($\sim$16 $\mu g/m^3$) (Figure S15, S17). This underestimation is likely related to the simplified aerosol representation in the current version of MAM4 used in MUSICAv0, which does not explicitly account for inorganic nitrate aerosols.[57,75]

To examine how MUSICAv0 captures the transport of fire plumes, Figure 7 shows the spatiotemporal evolution of the fire plume across northern England from 25 to 30 June, using CO as a tracer. CO is used as it is an inert tracer with a long atmospheric lifetime and low background concentrations over the study region. Throughout this period, meteorological conditions favor the development and spread of the fire plume. Northern England is dominated by a strong anticyclonic circulation at the 850 hPa level, resulting in a stable high-pressure system and associated low wind speeds that facilitate the aggregation of pollutants (Figure S14). Near the SM area, a notable temperature inversion is observed at 900 hPa, accompanied by significant near surface warming associated with the persistent high-pressure system (Figure 7g–l). The inversion strength increases by about 13 K at surface on 27 June compared to 24 June. At the same time, although strong descending motion generally inhibits the dispersion of pollutants during this period, stronger background ascending motion near the fire sites enhances the vertical mixing (Figure 7g–l).

Elevated CO concentrations are observed near the Saddleworth Moor on 25 June, with the fire plume extending southeastward (Figure 7a). As the anticyclone center shifts northeastward, regional meteorological conditions become increasingly favorable for pollutant accumulation, leading to peak concentrations across cities on 27 June (Figure 7c and Figure S14). These stagnant conditions also inhibit plume dispersion, resulting in relatively stationary smoke transport. Simulated CO concentrations reach around 400 ppbv in Manchester and Sheffield, with nearly 600 ppbv in Liverpool (Figure S19). Starting from 28 June, the gradual strengthening of northwesterly winds disrupts the anticyclonic circulation and weakens temperature inversion (4–7 K), thereby enhancing vertical mixing and horizontal transport, resulting in a rapid dispersion of the fire plume. Under such influence, pollutants are transported upward to the top of the planetary boundary layer, reaching altitudes approaching 500 hPa (Figures 7i–k and S14). At the same time, O_3 production is enhanced in downwind areas, consistent with previous findings,[27] with a 10.6% increase observed in Liverpool (Figures S19 and S18). The additional emissions released from the Winter Hill fire on 30 June[28] are uplifted by the prevailing winds and existing vertical mixing, facilitating long range transport of pollutants to downwind regions (Figure 7l). Overall, meteorological variability governs both the development and the subsequent dispersion of the fire plume. The Saddleworth Moor case study demonstrates the insights into the UK air quality that can be derived from MUSICAv0, in particular the role of wildfire on urban air quality, an issue expected to become increasingly important in the UK under future climate change.

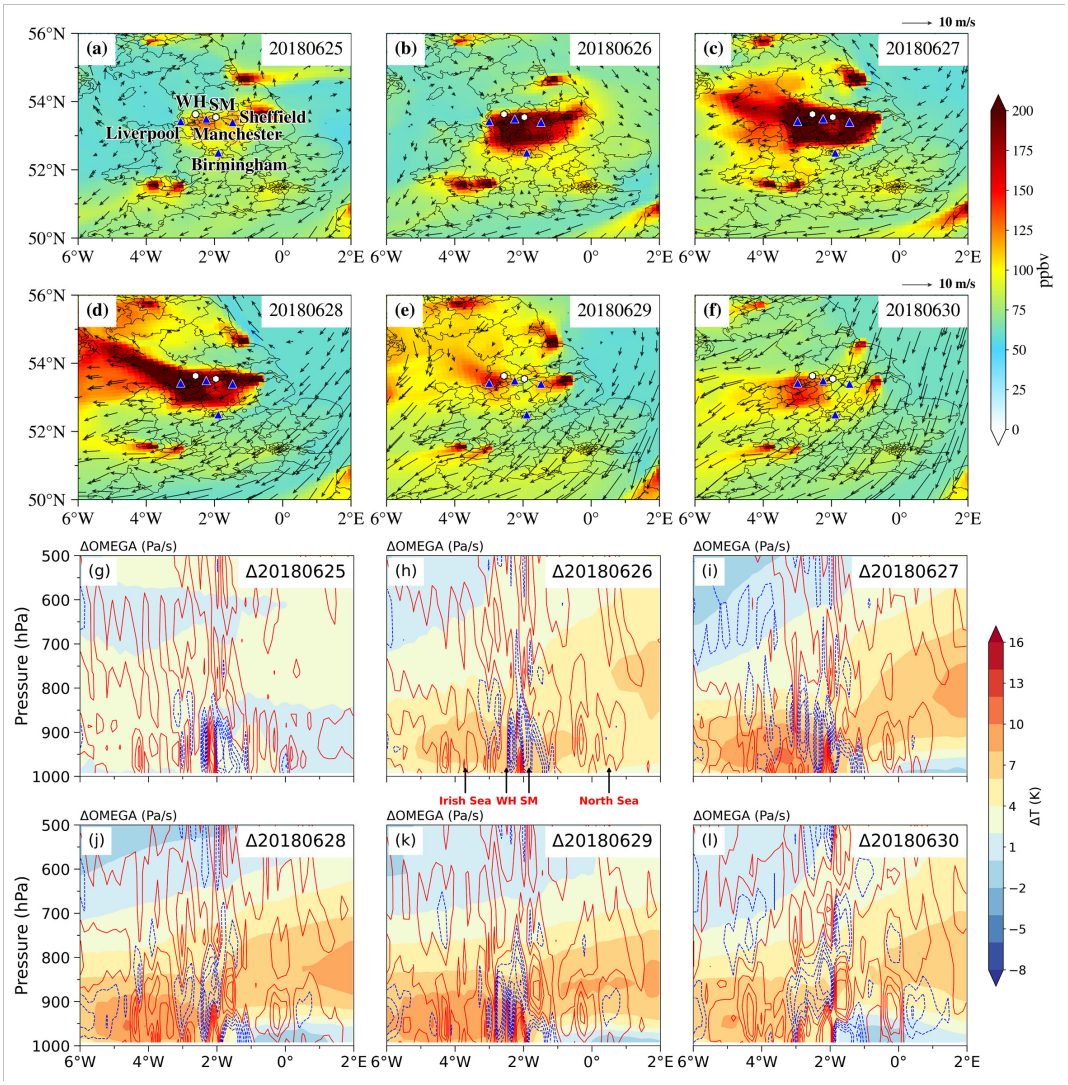

Figure 7: Surface daily CO concentrations (ppbv) over the southern UK (25–30 June 2018) with surface wind vectors represented by black arrows (a–f). White dots indicate the locations of the two fire sites: Winter Hill (WH) and Saddleworth Moor (SM), and blue triangles show selected cities. Panels (g–l) show west–east vertical cross sections at $53.40°N$ of changes in daily mean temperature (shaded; K) and vertical velocity (contoured; Pa/s; scaled by 100) for the same period, relative 24 June, 2018. Descending and ascending motions are represented by red solid contours and blue dashed contours, respectively. Red labels in panel (h) indicate the Irish Sea, WH, SM, and the North Sea.

4. DISCUSSION

Regional models are typically effective at resolving local air pollution processes, but often rely on boundary and initial conditions from GCMs or ESMs, which can introduce inconsistencies across spatial scales.[34,35] In this study, we develop a new UK regionally refined grid (UKne30×16; 1/16°) within MUSICAv0 to enable a consistent multi-scale assessment of BB impacts on UK air quality. The model performance and added value of this new configuration are assessed by comparison with the global uniform grid (ne60; 1/2°), the UKAQR dataset and surface AURN observations.

Evaluation against UKAQR demonstrates that MUSICAv0 with the UKne30×16 configuration reproduces the spatial patterns of surface O_3 and $PM_{2.5}$ across the UK. Agreement is strong for annual average O_3 (R = 0.87; NMB = 12.80%), while $PM_{2.5}$ spatial patterns are captured reasonably well (R = 0.64), albeit

with underestimation of concentrations in southeastern UK by about 2–4 $\mu g/m^3$ (NMB = -15.70%). This bias could be related to the omission of inorganic nitrate aerosols in the current MUSICAv0 configuration. The added value of the UK regional refinement is further shown during a late-spring continental pollution intrusion event. Compared with the global uniform grid, the UKne30×16 configuration more accurately reproduces observed $PM_{2.5}$ and O_3 variability when evaluated against AURN observations. The refined grid improves NSV by 8–20% for $PM_{2.5}$ and 5–10% for O_3, and produces $PM_{2.5}$ Sk values that more closely match observations, particularly in complex terrain such as Glasgow. These improvements are mostly attributed to better representation of fine-scale horizontal dispersion, vertical mixing, and an improved ability to resolve fine-scale chemical processes. In contrast, the ne60 configuration is affected by coarse resolution spatial averaging and the excessive accumulation of regional transport signals, leading to an overestimation of extreme pollution intrusion.

Building on this improved regional performance, we assess the influence of both global and regional BB on UK air quality. Global BB contributes substantially to seasonal $PM_{2.5}$ and O_3 across the UK, increasing $PM_{2.5}$ by 15–25% in Scotland and the eastern UK coast during spring and by 10–17% in central England during summer. Averaged over 2018, BB increases annual mean surface $PM_{2.5}$ over the UK by approximately 0.7 $\mu g/m^3$. Although modest in magnitude, this additional background contribution can substantially reduce the margin for meeting increasingly stringent air quality targets, such as the WHO guideline (5 $\mu g/m^3$) and the UK long-term $PM_{2.5}$ target of 10 $\mu g/m^3$ by 2040.[83,84] For O_3, BB enhancements reach approximately 12–14% in northwestern England and western Scotland during summer and expand across central Scotland and southwestern England during autumn, with fractional enhancements of 10–13%. These results highlight the importance of transboundary BB as a non-negligible contributor to UK air pollution, particularly during specific seasons and transport regimes. At the regional scale, the 2018 Saddleworth Moor wildfire provides a representative case study of domestic BB impacts. MUSICAv0 with the UKne30×16 configuration simulates a 133% enhancement in $PM_{2.5}$ over Manchester, consistent with previous studies,[28] although peak concentrations are slightly underestimated. Our configuration also captures enhanced downwind O_3 formation, with MDA8 O_3 increasing by 10.6% in Liverpool during the fire period. Changes in anticyclonic conditions contribute to both the formation and dispersion of the fire plumes, highlighting the important role of meteorology in controlling wildfire plume transport and air quality impacts.

However, this study has several limitations. Meteorological nudging is not applied within the refined domain (UKne30×16) due to its high-resolution, which may affect the representation of aerosol–meteorology feedbacks, relative to the globally nudged ne60 configuration. The simplified treatment of ammonium aerosols in our MAM4 version[57,75] limits the ability to fully represent nonlinear $PM_{2.5}$ formation, particularly in regions influenced by high NO_x emissions. In addition, uncertainties in fire emission estimates, including burned area, fuel load, and emission factors that vary with vegetation types, propagate into estimates of wildfire impacts.[69,85,86] Future work should consider the use of more detailed aerosol schemes such as the Model for Simulating Aerosol Interactions and Chemistry (MOSAIC) to more accurately represent nitrate aerosols,[87,88] and explicitly account for fires at the wildland–urban interfaces (WUI), which involve additional emissions from structure burning.

Overall, this study shows that biomass burning, both outside and within the UK, can make a substantial contribution to UK air pollution on seasonal and episodic events. These contributions often originate beyond national borders and are therefore difficult to control through domestic emission policies alone. The UK-specific MUSICA regional refinement developed provides a robust framework to quantify these external influences, linking global emissions, regional transport and local air quality. Beyond biomass burning, this new UK domain offers a flexible model for future studies of air quality, atmospheric composition, and climate-chemistry interactions under present and future climate conditions, while enabling urban-scale air pollution to be interpreted consistently within its regional and global context.

Data Availability Statement

MUSICAv0[43] is a configuration of CESM2.2, which is an open-source community model available at `https://github.com/ESCOMP/CESM` [Software]. The CAMS-GLOB-ANTv5.1 and CAMS-GLOB-AIRv2.1[67,89] emission inventories are available from the Emissions of atmospheric Compounds and Compilation of Ancillary Data (ECCAD) database (`https://eccad.aeris-data.fr` [Data]). The AURN ground-based air quality

observations are available at https://uk-air.defra.gov.uk/networks/network-info?view=aurn [Data]. The UKAQR reanalysis data are provided by the Met Office (https://air-quality-1-themetoffice.hub.arcgis.com/pages/explore-data [Data]).

Acknowledgements

This work was supported by the Royal Society (grant numbers RG\R1\251567). This work used the ARCHER2 UK National Supercomputing Service (https://www.archer2.ac.uk). The authors acknowledge the assistance given by Research IT, and the use of The HPC Pool funded by the Research Lifecycle Programme at The University of Manchester. MVM acknowledges fundings from the United Kingdom Research and Innovation (UKRI) Future Leaders Fellowship (grant numbers MR/T019867/1 and UKRI2059).

References

[1] Cohen, A. J. et al. Estimates and 25-Year Trends of the Global Burden of Disease Attributable to Ambient Air Pollution: An Analysis of Data from the Global Burden of Diseases Study 2015. *The Lancet* **2017**, *389*, 1907–1918, DOI: 10.1016/S0140-6736(17)30505-6.

[2] Apte, J. S.; Messier, K. P.; Gani, S.; Brauer, M.; Kirchstetter, T. W.; Lunden, M. M.; Marshall, J. D.; Portier, C. J.; Vermeulen, R. C.; Hamburg, S. P. High-Resolution Air Pollution Mapping with Google Street View Cars: Exploiting Big Data. *Environmental Science & Technology* **2017**, *51*, 6999–7008, DOI: 10.1021/acs.est.7b00891.

[3] Apte, J. S.; Marshall, J. D.; Cohen, A. J.; Brauer, M. Addressing Global Mortality from Ambient PM2.5. *Environmental Science & Technology* **2015**, *49*, 8057–8066, DOI: 10.1021/acs.est.5b01236.

[4] Macintyre, H. L.; Mitsakou, C.; Thompson, S.; Aldridge, S.; Exley, K. S.; Guercio, V.; Heal, M. R.; Vieno, M.; Heaviside, C. *Health Effects of Climate Change (HECC) in the UK: 2023 report*; UK Health Security Agency, 2023.

[5] Das, D.; Ahmad, S.; Kirshner, J. Opportunities and Challenges Associated with the Uptake of Residential Clean Fuel Usage. *Current Environmental Health Reports* **2024**, *11*, 204–209, DOI: 10.1007/s40572-024-00438-7.

[6] Andreae, M. O.; Merlet, P. Emission of Trace Gases and Aerosols from Biomass Burning. *Global Biogeochemical Cycles* **2001**, *15*, 955–966, DOI: 10.1029/2000GB001382.

[7] Bikkina, S.; Haque, M. M.; Sarin, M.; Kawamura, K. Tracing the Relative Significance of Primary versus Secondary Organic Aerosols from Biomass Burning Plumes over Coastal Ocean Using Sugar Compounds and Stable Carbon Isotopes. *ACS Earth and Space Chemistry* **2019**, *3*, 1471–1484, DOI: 10.1021/acsearthspacechem.9b00140.

[8] Jimenez, J. L. et al. Evolution of Organic Aerosols in the Atmosphere. *Science* **2009**, *326*, 1525–1529, DOI: 10.1126/science.1180353.

[9] Majdi, M.; Sartelet, K.; Lanzafame, G. M.; Couvidat, F.; Kim, Y.; Chrit, M.; Turquety, S. Precursors and Formation of Secondary Organic Aerosols from Wildfires in the Euro-Mediterranean Region. *Atmospheric Chemistry and Physics* **2019**, *19*, 5543–5569, DOI: 10.5194/acp-19-5543-2019.

[10] Lim, C. Y.; Hagan, D. H.; Coggon, M. M.; Koss, A. R.; Sekimoto, K.; de Gouw, J.; Warneke, C.; Cappa, C. D.; Kroll, J. H. Secondary Organic Aerosol Formation from the Laboratory Oxidation of Biomass Burning Emissions. *Atmospheric Chemistry and Physics* **2019**, *19*, 12797–12809, DOI: 10.5194/acp-19-12797-2019.

[11] Yadav, I. C.; Linthoingambi Devi, N.; Li, J.; Syed, J. H.; Zhang, G.; Watanabe, H. Biomass Burning in Indo-China Peninsula and Its Impacts on Regional Air Quality and Global Climate Change-a Review. *Environmental Pollution* **2017**, *227*, 414–427, DOI: 10.1016/j.envpol.2017.04.085.

[12] Wan, N.; Xiong, X.; Kluitenberg, G. J.; Hutchinson, J. M. S.; Aiken, R.; Zhao, H.; Lin, X. Estimation of Biomass Burning Emission of NO_2 and CO from 2019–2020 Australia Fires Based on Satellite Observations. *Atmospheric Chemistry and Physics* **2023**, *23*, 711–724, DOI: 10.5194/acp-23-711-2023.

[13] Rogers, H. M.; Ditto, J. C.; Gentner, D. R. Evidence for Impacts on Surface-Level Air Quality in the Northeastern US from Long-Distance Transport of Smoke from North American Fires during the Long Island Sound Tropospheric Ozone Study (LISTOS) 2018. *Atmospheric Chemistry and Physics* **2020**, *20*, 671–682, DOI: 10.5194/acp-20-671-2020.

[14] Cordell, R. L.; Mazet, M.; Dechoux, C.; Hama, S. M. L.; Staelens, J.; Hofman, J.; Stroobants, C.; Roekens, E.; Kos, G. P. A.; Weijers, E. P.; Frumau, K. F. A.; Panteliadis, P.; Delaunay, T.; Wyche, K. P.; Monks, P. S. Evaluation of Biomass Burning across North West Europe and Its Impact on Air Quality. *Atmospheric Environment* **2016**, *141*, 276–286, DOI: 10.1016/j.atmosenv.2016.06.065.

[15] McClure, C. D.; Jaffe, D. A. Investigation of High Ozone Events Due to Wildfire Smoke in an Urban Area. *Atmospheric Environment* **2018**, *194*, 146–157, DOI: 10.1016/j.atmosenv.2018.09.021.

[16] Martins, L. D.; Hallak, R.; Alves, R. C.; de Almeida, D. S.; Squizzato, R.; Moreira, C. A. B.; Beal, A.; da Silva, I.; Rudke, A.; Martins, J. A. Long-Range Transport of Aerosols from Biomass Burning over Southeastern South America and Their Implications on Air Quality. *Aerosol and Air Quality Research* **2018**, *18*, 1734–1745, DOI: 10.4209/aaqr.2017.11.0545.

[17] Hu, Q.; Goloub, P.; Veselovskii, I.; Podvin, T. The Characterization of Long-Range Transported North American Biomass Burning Plumes: What Can a Multi-Wavelength Mie–Raman-polarization-fluorescence Lidar Provide? *Atmospheric Chemistry and Physics* **2022**, *22*, 5399–5414, DOI: 10.5194/acp-22-5399-2022.

[18] Masoom, A.; Kazadzis, S.; Modini, R. L.; Gysel-Beer, M.; Gröbner, J.; Coen, M. C.; Navas-Guzman, F.; Kouremeti, N.; Brem, B. T.; Nowak, N. K.; Martucci, G.; Hervo, M.; Erb, S. Long Range Transport of Canadian Wildfire Smoke to Europe in Fall 2023: Aerosol Properties and Spectral Features of Smoke Particles. *EGUsphere* **2025**, *2025*, 1–43, DOI: 10.5194/egusphere-2025-2755.

[19] Schollaert, C.; Connolly, R.; Cushing, L.; Jerrett, M.; Liu, T.; Marlier, M. Air Quality Impacts of the January 2025 Los Angeles Wildfires: Insights from Public Data Sources. *Environmental Science & Technology Letters* **2025**, *12*, 911–917, DOI: 10.1021/acs.estlett.5c00486.

[20] Rodrigues, M.; Mariani, M.; Russo, A.; Salis, M.; Galizia, L. F.; Cardil, A. Spatio-Temporal Domains of Wildfire-Prone Teleconnection Patterns in the Western Mediterranean Basin. *Geophysical Research Letters* **2021**, *48*, e2021GL094238, DOI: https://doi.org/10.1029/2021GL094238.

[21] Val Martin, M.; Kahn, R. A.; Tosca, M. G. A Global Analysis of Wildfire Smoke Injection Heights Derived from Space-Based Multi-Angle Imaging. *Remote Sensing* **2018**, *10*, 1609, DOI: 10.3390/rs10101609.

[22] Val Martin, M.; Honrath, R. E.; Owen, R. C.; Lapina, K. Large-scale impacts of anthropogenic pollution and boreal wildfires on the nitrogen oxides over the central North Atlantic region. *Journal of Geophysical Research: Atmospheres* **2008**, *113*, DOI: https://doi.org/10.1029/2007JD009689.

[23] Ansmann, A.; Baars, H.; Chudnovsky, A.; Mattis, I.; Veselovskii, I.; Haarig, M.; Seifert, P.; Engelmann, R.; Wandinger, U. Extreme Levels of Canadian Wildfire Smoke in the Stratosphere over Central Europe on 21–22 August 2017. *Atmospheric Chemistry and Physics* **2018**, *18*, 11831–11845, DOI: 10.5194/acp-18-11831-2018.

[24] Tan, D. Y. T.; Heal, M. R.; Stevenson, D. S.; Reis, S.; Vieno, M.; Nemitz, E. Long-Range Impacts of Biomass Burning on PM2.5: A Case Study of the UK with a Globally Nested Model. *EGUsphere* **2025**, DOI: 10.5194/egusphere-2025-5524.

[25] Lane, R. A.; Kay, A. L. Climate Change Impact on the Magnitude and Timing of Hydrological Extremes Across Great Britain. *Frontiers in Water* **2021**, *3*, DOI: 10.3389/frwa.2021.684982.

[26] Hanlon, H. M.; Bernie, D.; Carigi, G.; Lowe, J. A. Future Changes to High Impact Weather in the UK. *Climatic Change* **2021**, *166*, 50, DOI: 10.1007/s10584-021-03100-5.

[27] Graham, A. M. et al. Impact of the June 2018 Saddleworth Moor Wildfires on Air Quality in Northern England. *Environmental Research Communications* **2020**, *2*, 031001, DOI: 10.1088/2515-7620/ab7b92.

[28] Graham, A. M.; Pope, R. J.; Pringle, K. P.; Arnold, S.; Chipperfield, M. P.; Conibear, L. A.; Butt, E. W.; Kiely, L.; Knote, C.; McQuaid, J. B. Impact on Air Quality and Health Due to the Saddleworth Moor Fire in Northern England. *Environmental Research Letters* **2020**, *15*, 074018, DOI: 10.1088/1748-9326/ab8496.

[29] Baró, R.; Lorente-Plazas, R.; Montávez, J. P.; Jiménez-Guerrero, P. Biomass Burning Aerosol Impact on Surface Winds during the 2010 Russian Heat Wave. *Geophysical Research Letters* **2017**, *44*, 1088–1094, DOI: 10.1002/2016GL071484.

[30] Zauli-Sajani, S.; Thunis, P.; Pisoni, E.; Bessagnet, B.; Monforti-Ferrario, F.; De Meij, A.; Pekar, F.; Vignati, E. Reducing Biomass Burning Is Key to Decrease PM2.5 Exposure in European Cities. *Scientific Reports* **2024**, *14*, 10210, DOI: 10.1038/s41598-024-60946-2.

[31] Jiang, J.; El Haddad, I.; Aksoyoglu, S.; Stefenelli, G.; Bertrand, A.; Marchand, N.; Canonaco, F.; Petit, J.-E.; Favez, O.; Gilardoni, S.; Baltensperger, U.; Prévôt, A. S. H. Influence of Biomass Burning Vapor Wall Loss Correction on Modeling Organic Aerosols in Europe by CAMx v6.50. *Geoscientific Model Development* **2021**, *14*, 1681–1697, DOI: 10.5194/gmd-14-1681-2021.

[32] Li, X.; Han, J.; Hopke, P. K.; Hu, J.; Shu, Q.; Chang, Q.; Ying, Q. Quantifying Primary and Secondary Humic-like Substances in Urban Aerosol Based on Emission Source Characterization and a Source-Oriented Air Quality Model. *Atmospheric Chemistry and Physics* **2019**, *19*, 2327–2341, DOI: 10.5194/acp-19-2327-2019.

[33] Hood, C.; MacKenzie, I.; Stocker, J.; Johnson, K.; Carruthers, D.; Vieno, M.; Doherty, R. Air quality simulations for London using a coupled regional-to-local modelling system. *Atmospheric Chemistry and Physics* **2018**, *18*, 11221–11245, DOI: 10.5194/acp-18-11221-2018.

[34] Carter, J.; Leeson, A.; Orr, A.; Kittel, C.; van Wessem, J. M. Variability in Antarctic Surface Climatology across Regional Climate Models and Reanalysis Datasets. *The Cryosphere* **2022**, *16*, 3815–3841, DOI: 10.5194/tc-16-3815-2022.

[35] Ambrizzi, T.; Reboita, M. S.; da Rocha, R. P.; Llopart, M. The State of the Art and Fundamental Aspects of Regional Climate Modeling in South America. *Annals of the New York Academy of Sciences* **2019**, *1436*, 98–120, DOI: 10.1111/nyas.13932.

[36] Gettelman, A.; Callaghan, P.; Larson, V. E.; Zarzycki, C. M.; Bacmeister, J. T.; Lauritzen, P. H.; Bogenschutz, P. A.; Neale, R. B. Regional Climate Simulations With the Community Earth System Model. *Journal of Advances in Modeling Earth Systems* **2018**, *10*, 1245–1265, DOI: 10.1002/2017MS001227.

[37] Giorgi, F. Thirty Years of Regional Climate Modeling: Where Are We and Where Are We Going Next? *Journal of Geophysical Research: Atmospheres* **2019**, *124*, 5696–5723, DOI: 10.1029/2018JD030094.

[38] Singh, V.; Jain, S. K.; Singh, P. K. Inter-Comparisons and Applicability of CMIP5 GCMs, RCMs and Statistically Downscaled NEX-GDDP Based Precipitation in India. *Science of The Total Environment* **2019**, *697*, 134163, DOI: 10.1016/j.scitotenv.2019.134163.

[39] Joseph, J.; Ghosh, S.; Pathak, A.; Sahai, A. K. Hydrologic Impacts of Climate Change: Comparisons between Hydrological Parameter Uncertainty and Climate Model Uncertainty. *Journal of Hydrology* **2018**, *566*, 1–22, DOI: 10.1016/j.jhydrol.2018.08.080.

[40] Cha, D.-H.; Jin, C.-S.; Moon, J.-H.; Lee, D.-K. Improvement of Regional Climate Simulation of East Asian Summer Monsoon by Coupled Air-Sea Interaction and Large-Scale Nudging: IMPROVEMENT OF EASM SIMULATION BY AIR-SEA COUPLING AND NUDGING. *International Journal of Climatology* **2016**, *36*, 334–345, DOI: 10.1002/joc.4349.

[41] Syed, F. S.; Iqbal, W.; Syed, A. A. B.; Rasul, G. Uncertainties in the Regional Climate Models Simulations of South-Asian Summer Monsoon and Climate Change. *Climate Dynamics* **2014**, *42*, 2079–2097, DOI: 10.1007/s00382-013-1963-x.

[42] Xu, Z.; Chang, A.; Di Vittorio, A. Evaluating and Projecting of Climate Extremes Using a Variable-Resolution Global Climate Model (VR-CESM). *Weather and Climate Extremes* **2022**, *38*, 100496, DOI: 10.1016/j.wace.2022.100496.

[43] Pfister, G. G. et al. The Multi-Scale Infrastructure for Chemistry and Aerosols (MUSICA). *Bulletin of the American Meteorological Society* **2020**, *101*, E1743–E1760, DOI: 10.1175/BAMS-D-19-0331.1.

[44] Tang, W. et al. Disproportionately Large Impacts of Wildland-Urban Interface Fire Emissions on Global Air Quality and Human Health. *Science Advances* **2025**, *11*, eadr2616, DOI: 10.1126/sciadv.adr2616.

[45] Lichtig, P.; Gaubert, B.; Emmons, L. K.; Jo, D. S.; Callaghan, P.; Ibarra-Espinosa, S.; Dawidowski, L.; Brasseur, G. P.; Pfister, G. Multiscale CO Budget Estimates Across South America: Quantifying Local Sources and Long Range Transport. *Journal of Geophysical Research: Atmospheres* **2024**, *129*, e2023JD040434, DOI: 10.1029/2023JD040434.

[46] Yue, M.; Dong, X.; Wang, M.; Emmons, L. K.; Liang, Y.; Tong, D.; Liu, Y.; Liu, Y. Modeling the Air Pollution and Aerosol-PBL Interactions Over China Using a Variable-Resolution Global Model. *Journal of Geophysical Research: Atmospheres* **2023**, *128*, e2023JD039130, DOI: 10.1029/2023JD039130.

[47] Jo, D. S. et al. Comparison of Urban Air Quality Simulations During the KORUS-AQ Campaign With Regionally Refined Versus Global Uniform Grids in the Multi-Scale Infrastructure for Chemistry and Aerosols (MUSICA) Version 0. *Journal of Advances in Modeling Earth Systems* **2023**, *15*, e2022MS003458, DOI: 10.1029/2022MS003458.

[48] Danabasoglu, G. et al. The Community Earth System Model Version 2 (CESM2). *Journal of Advances in Modeling Earth Systems* **2020**, *12*, e2019MS001916, DOI: 10.1029/2019MS001916.

[49] Lauritzen, P. H. et al. NCAR Release of CAM-SE in CESM2.0: A Reformulation of the Spectral Element Dynamical Core in Dry-Mass Vertical Coordinates With Comprehensive Treatment of Condensates and Energy. *Journal of Advances in Modeling Earth Systems* **2018**, *10*, 1537–1570, DOI: 10.1029/2017MS001257.

[50] Danabasoglu, G. et al. The Community Earth System Model Version 2 (CESM2). *Journal of Advances in Modeling Earth Systems* **2020**, *12*, e2019MS001916, DOI: 10.1029/2019MS001916.

[51] Tilmes, S.; Hodzic, A.; Emmons, L. K.; Mills, M. J.; Gettelman, A.; Kinnison, D. E.; Park, M.; Lamarque, J.-F.; Vitt, F.; Shrivastava, M.; Campuzano-Jost, P.; Jimenez, J. L.; Liu, X. Climate Forcing and Trends of Organic Aerosols in the Community Earth System Model (CESM2). *Journal of Advances in Modeling Earth Systems* **2019**, *11*, 4323–4351, DOI: 10.1029/2019MS001827.

[52] Tang, W.; Pfister, G. G.; Kumar, R.; Barth, M.; Edwards, D. P.; Emmons, L. K.; Tilmes, S. Capturing High-Resolution Air Pollution Features Using the Multi-Scale Infrastructure for Chemistry and Aerosols Version 0 (MUSICAv0) Global Modeling System. *Journal of Geophysical Research: Atmospheres* **2023**, *128*, e2022JD038345, DOI: https://doi.org/10.1029/2022JD038345.

[53] Schwantes, R. H. et al. Evaluating the Impact of Chemical Complexity and Horizontal Resolution on Tropospheric Ozone Over the Conterminous US With a Global Variable Resolution Chemistry Model. *Journal of Advances in Modeling Earth Systems* **2022**, *14*, e2021MS002889, DOI: 10.1029/2021MS002889.

[54] Bogenschutz, P. A.; Gettelman, A.; Morrison, H.; Larson, V. E.; Craig, C.; Schanen, D. P. Higher-Order Turbulence Closure and Its Impact on Climate Simulations in the Community Atmosphere Model. *Journal of Climate* **2013**, *26*, 9655–9676, DOI: 10.1175/JCLI-D-13-00075.1.

[55] Golaz, J.-C.; Larson, V. E.; Cotton, W. R. A PDF-Based Model for Boundary Layer Clouds. Part I: Method and Model Description. *Journal of the Atmospheric Sciences* **2002**, *59*, 3540–3551, DOI: 10.1175/1520-0469(2002)059<3540:APBMFB>2.0.CO;2.

[56] Lawrence, D. M. et al. The Community Land Model Version 5: Description of New Features, Benchmarking, and Impact of Forcing Uncertainty. *Journal of Advances in Modeling Earth Systems* **2019**, *11*, 4245–4287, DOI: 10.1029/2018MS001583.

[57] Liu, X.; Ma, P.-L.; Wang, H.; Tilmes, S.; Singh, B.; Easter, R. C.; Ghan, S. J.; Rasch, P. J. Description and Evaluation of a New Four-Mode Version of the Modal Aerosol Module (MAM4) within Version 5.3 of the Community Atmosphere Model. *Geoscientific Model Development* **2016**, *9*, 505–522, DOI: 10.5194/gmd-9-505-2016.

[58] Zhang, G.; McFarlane, N. A. Sensitivity of Climate Simulations to the Parameterization of Cumulus Convection in the Canadian Climate Centre General Circulation Model. *Atmosphere-Ocean* **1995**, *33*, 407–446, DOI: 10.1080/07055900.1995.9649539.

[59] Lawrence, D. M.; Fisher, R. A.; Koven, C. D.; Oleson, K. W.; Swenson, S. C.; Bonan, G.; Collier, N.; Ghimire, B.; Van Kampenhout, L.; Kennedy, D.; others The Community Land Model version 5: Description of new features, benchmarking, and impact of forcing uncertainty. *Journal of Advances in Modeling Earth Systems* **2019**, *11*, 4245–4287.

[60] Schwantes, R. H.; Emmons, L. K.; Orlando, J. J.; Barth, M. C.; Tyndall, G. S.; Hall, S. R.; Ullmann, K.; St. Clair, J. M.; Blake, D. R.; Wisthaler, A.; Bui, T. P. V. Comprehensive Isoprene and Terpene Gas-Phase Chemistry Improves Simulated Surface Ozone in the Southeastern US. *Atmospheric Chemistry and Physics* **2020**, *20*, 3739–3776, DOI: 10.5194/acp-20-3739-2020.

[61] Lauritzen, P. H.; Jablonowski, C.; Taylor, M. A.; Nair, R. D. Rotated Versions of the Jablonowski Steady-State and Baroclinic Wave Test Cases: A Dynamical Core Intercomparison. *Journal of Advances in Modeling Earth Systems* **2010**, *2*, DOI: 10.3894/JAMES.2010.2.15.

[62] Herrington, A. R.; Reed, K. A. On Resolution Sensitivity in the Community Atmosphere Model. *Quarterly Journal of the Royal Meteorological Society* **2020**, *146*, 3789–3807, DOI: 10.1002/qj.3873.

[63] Guenther, A. B.; Jiang, X.; Heald, C. L.; Sakulyanontvittaya, T.; Duhl, T.; Emmons, L. K.; Wang, X. The Model of Emissions of Gases and Aerosols from Nature Version 2.1 (MEGAN2.1): An Extended and Updated Framework for Modeling Biogenic Emissions. *Geoscientific Model Development* **2012**, *5*, 1471–1492, DOI: 10.5194/gmd-5-1471-2012.

[64] Price, C.; Penner, J.; Prather, M. NOx from lightning: 1. Global distribution based on lightning physics. *Journal of Geophysical Research: Atmospheres* **1997**, *102*, 5929–5941, DOI: https://doi.org/10.1029/96JD03504.

[65] Crippa, M.; Oreggioni, G.; Muntean, M.; schaaf, e.; Vullo, E.; Solazzo, E.; Monforti, F.; Olivier, J.; Vignati, E. *EDGAR Booklet 2019*; 2019; DOI: 10.2760/655913.

[66] McDuffie, E. E.; Smith, S. J.; O'Rourke, P.; Tibrewal, K.; Venkataraman, C.; Marais, E. A.; Zheng, B.; Crippa, M.; Brauer, M.; Martin, R. V. A Global Anthropogenic Emission Inventory of Atmospheric Pollutants from Sector- and Fuel-Specific Sources (1970–2017): An Application of the Community Emissions Data System (CEDS). *Earth System Science Data* **2020**, *12*, 3413–3442, DOI: 10.5194/essd-12-3413-2020.

[67] Granier, C.; Darras, S.; Denier van Der Gon, H.; Jana, D.; Elguindi, N.; Bo, G.; Michael, G.; Marc, G.; Jalkanen, J.-P.; Kuenen, J.; Liousse, C.; Quack, B.; Simpson, D.; Sindelarova, K. *The Copernicus Atmosphere Monitoring Service global and regional emissions (April 2019 version)*; Research Report, 2019; DOI: 10.24380/d0bn-kx16.

[68] Koster, R. D.; Darmenov, A. S.; Silva, A. D. The Quick Fire Emissions Dataset (QFED): Documentation of Versions 2.1, 2.2 and 2.4. Volume 38; Technical Report Series on Global Modeling and Data Assimilation. 2015.

[69] Wiedinmyer, C.; Akagi, S. K.; Yokelson, R. J.; Emmons, L. K.; Al-Saadi, J. A.; Orlando, J. J.; Soja, A. J. The Fire INventory from NCAR (FINN): A High Resolution Global Model to Estimate the Emissions from Open Burning. *Geoscientific Model Development* **2011**, *4*, 625–641, DOI: 10.5194/gmd-4-625-2011.

[70] Tilmes, S.; Lamarque, J.-F.; Emmons, L. K.; Kinnison, D. E.; Marsh, D.; Garcia, R. R.; Smith, A. K.; Neely, R. R.; Conley, A.; Vitt, F.; Val Martin, M.; Tanimoto, H.; Simpson, I.; Blake, D. R.; Blake, N. Representation of the Community Earth System Model (CESM1) CAM4-chem within the Chemistry-Climate Model Initiative (CCMI). *Geoscientific Model Development* **2016**, *9*, 1853–1890, DOI: 10.5194/gmd-9-1853-2016.

[71] Jones, P. W. First- and Second-Order Conservative Remapping Schemes for Grids in Spherical Coordinates. *Monthly Weather Review* **1999**, *127*, 2204–2210, DOI: 10.1175/1520-0493(1999)127<2204:FASOCR>2.0.CO;2.

[72] van Wees, D.; van der Werf, G. R.; Randerson, J. T.; Rogers, B. M.; Chen, Y.; Veraverbeke, S.; Giglio, L.; Morton, D. C. Global Biomass Burning Fuel Consumption and Emissions at 500 m Spatial Resolution Based on the Global Fire Emissions Database (GFED). *Geoscientific Model Development* **2022**, *15*, 8411–8437, DOI: 10.5194/gmd-15-8411-2022.

[73] Gelaro, R. et al. The Modern-Era Retrospective Analysis for Research and Applications, Version 2 (MERRA-2). *Journal of Climate* **2017**, *30*, 5419–5454, DOI: 10.1175/JCLI-D-16-0758.1.

[74] Tao, M.; Fiore, A. M.; Emmons, L. K.; Scott, J. R.; Pfister, G. G.; Jo, D. S.; Tang, W. Contrasting Air Pollution Responses to Hourly Varying Anthropogenic NO_x Emissions in the Contiguous United States. *EGUsphere* **2025**, 1–33, DOI: 10.5194/egusphere-2025-4304.

[75] Liu, X. et al. Toward a Minimal Representation of Aerosols in Climate Models: Description and Evaluation in the Community Atmosphere Model CAM5. *Geoscientific Model Development* **2012**, *5*, 709–739, DOI: 10.5194/gmd-5-709-2012.

[76] Tan, D. Y. T.; Heal, M. R.; Vieno, M.; Stevenson, D. S.; Reis, S.; Nemitz, E. Changes in Atmospheric Oxidants Teleconnect Biomass Burning and Ammonium Nitrate Formation. *npj Climate and Atmospheric Science* **2025**, *8*, 277, DOI: 10.1038/s41612-025-01150-5.

[77] Srivastava, D.; Saksakulkrai, S.; Acton, W. J. F.; Rooney, D. J.; Hall, J.; Hou, S.; Wolstencroft, M.; Bartington, S.; Harrison, R. M.; Shi, Z.; Bloss, W. J. Comparative Receptor Modelling for the Sources of Fine Particulate Matter (PM2.5) at Urban Sites in the UK. *Atmospheric Environment* **2025**, *343*, 120963, DOI: 10.1016/j.atmosenv.2024.120963.

[78] Vieno, M.; Heal, M. R.; Hallsworth, S.; Famulari, D.; Doherty, R. M.; Dore, A. J.; Tang, Y. S.; Braban, C. F.; Leaver, D.; Sutton, M. A.; Reis, S. The Role of Long-Range Transport and Domestic Emissions in Determining Atmospheric Secondary Inorganic Particle Concentrations across the UK. *Atmospheric Chemistry and Physics* **2014**, *14*, 8435–8447, DOI: 10.5194/acp-14-8435-2014.

[79] Wang, W.; Fecht, D.; Beevers, S.; Gulliver, J. Predicting Daily Concentrations of Nitrogen Dioxide, Particulate Matter and Ozone at Fine Spatial Scale in Great Britain. *Atmospheric Pollution Research* **2022**, *13*, 101506, DOI: 10.1016/j.apr.2022.101506.

[80] Diaz, F. M. R.; Khan, M. A. H.; Shallcross, B. M. A.; Shallcross, E. D. G.; Vogt, U.; Shallcross, D. E. Ozone Trends in the United Kingdom over the Last 30 Years. *Atmosphere* **2020**, *11*, 534, DOI: 10.3390/atmos11050534.

[81] Romero-Alvarez, J.; Lupaşcu, A.; Lowe, D.; Badia, A.; Archer-Nicholls, S.; Dorling, S.; Reeves, C. E.; Butler, T. Sources of Surface O_3 in the UK: Tagging O_3 within WRF-chem. *Atmospheric Chemistry and Physics* **2022**, *22*, 13797–13815, DOI: 10.5194/acp-22-13797-2022.

[82] Drummond, B.; Graham, A.; Neal, L.; Jiménez, P. M.; Pope, R. J.; Reddington, C. Air Quality Impacts of a Major Wildfire in the UK: Sensitivity to Model Spatial Resolution and Transport Method. *Atmospheric Pollution Research* **2026**, *17*, 102795, DOI: 10.1016/j.apr.2025.102795.

[83] Organization, W. H. *WHO global air quality guidelines: particulate matter (PM2. 5 and PM10), ozone, nitrogen dioxide, sulfur dioxide and carbon monoxide*; World Health Organization, 2021.

[84] Department for Environment, Food and Rural Affairs DEFRA Air Quality Targets in the Environment Act. 2023; https://uk-air.defra.gov.uk/networks/monitoring-methods.

[85] van der Werf, G. R.; Randerson, J. T.; Giglio, L.; van Leeuwen, T. T.; Chen, Y.; Rogers, B. M.; Mu, M.; van Marle, M. J. E.; Morton, D. C.; Collatz, G. J.; Yokelson, R. J.; Kasibhatla, P. S. Global Fire Emissions Estimates during 1997–2016. *Earth System Science Data* **2017**, *9*, 697–720, DOI: 10.5194/essd-9-697-2017.

[86] He, C.; Kumar, R.; Tang, W.; Pfister, G.; Xu, Y.; Qian, Y.; Brasseur, G. Air Pollution Interactions with Weather and Climate Extremes: Current Knowledge, Gaps, and Future Directions. *Current Pollution Reports* **2024**, *10*, 430–442, DOI: 10.1007/s40726-024-00296-9.

[87] Lu, Z.; Liu, X.; Zaveri, R. A.; Easter, R. C.; Tilmes, S.; Emmons, L. K.; Vitt, F.; Singh, B.; Wang, H.; Zhang, R.; Rasch, P. J. Radiative Forcing of Nitrate Aerosols From 1975 to 2010 as Simulated by MOSAIC Module in CESM2-MAM4. *Journal of Geophysical Research: Atmospheres* **2021**, *126*, e2021JD034809, DOI: 10.1029/2021JD034809.

[88] Zaveri, R. A.; Easter, R. C.; Singh, B.; Wang, H.; Lu, Z.; Tilmes, S.; Emmons, L. K.; Vitt, F.; Zhang, R.; Liu, X.; Ghan, S. J.; Rasch, P. J. Development and Evaluation of Chemistry-Aerosol-Climate Model CAM5-Chem-MAM7-MOSAIC: Global Atmospheric Distribution and Radiative Effects of Nitrate Aerosol. *Journal of Advances in Modeling Earth Systems* **2021**, *13*, e2020MS002346, DOI: 10.1029/2020MS002346.

[89] Elguindi, N. et al. Intercomparison of Magnitudes and Trends in Anthropogenic Surface Emissions From Bottom-Up Inventories, Top-Down Estimates, and Emission Scenarios. *Earth's Future* **2020**, *8*, e2020EF001520, DOI: 10.1029/2020EF001520.